Luminosity function of binary X-ray sources calculated using the Scenario Machine

A.I. Bogomazov
Sternberg astronomical institute, 119992, Universitetskij prospect, 13, Moscow, Russia
a78b@yandex.ru

V.M. Lipunov
Sternberg astronomical institute, 119992, Universitetskij prospect, 13, Moscow, Russia
lipunov@xray.sai.msu.ru

ABSTRACT

Using the "Scenario Machine" we have carried out a population synthesis of X-ray binaries for the purpose of modelling of X-ray luminosity functions (XLFs) in different types of galaxies: star burst, spiral, and elliptical. This computer code allows to calculate, by using Monte Carlo simulations, the evolution of a large ensemble of binary systems, with proper accounting for the spin evolution of magnetized neutron stars.

We show that the XLF has no universal type. It depends on the star formation rate in the galaxy. Also it is of importance to take into account the evolution of binary systems and life times of X-ray stages in theoretical models of such functions. We have calculated cumulative and differential XLFs for the galaxy with the constant star formation rate. Also we have calculated cumulative luminosity functions for different intervals of time after the star formation burst in the galaxy and curves depicting the evolution of the X-ray luminosity after the star formation burst in the galaxy.

Subject headings: binaries: close — binaries: general — X-rays: binaries — X-rays: general

1. INTRODUCTION

The evolution of the X-ray luminosity of galaxies was predicted by Tatarinzeva et al. (1989)[1]. They studied X-rays come from X-ray binary stars. The evolution of the X-ray luminosity $L_\delta(t)$ was calculated assuming the δ-function shape for the star formation rate (simultaneous birth of the stars). The evolution of the X-ray luminosity of the galaxy with an arbitrary star formation rate $\phi(t)$ can be represented as

$$L(t) = \int_{-\infty}^{+\infty} L_\delta(t-\tau)\phi(\tau)\,d\tau, \qquad (1)$$

The evolution of the total X-ray luminosity after $t > 2 \times 10^9$ years (long time scale) from the star formation burst can be well fitted by power law (Tatarinzeva et al. 1989)[1]:

$$L(t) \approx 3{\cdot}10^{40} \left(\frac{N}{10^{12}}\right) \left(\frac{t}{10^9 \mathrm{yr}}\right)^{-1.56} \mathrm{erg{\cdot}s^{-1}}, \quad (2)$$

here N is the total number of the stars in the galaxy.

Lipunov et al. (1996a) studied the evolution of stellar populations after the star formation burst occurring in the conditions similar to the Milky Way, in the central part of the galaxy, on a timescale of 10 Myr. Their results include a number of X-ray transients (each consisting of a neutron star and a main sequence star), super accreting black holes, and binaries consisting of a

[1]See also Lipunov et al. (1996b)

black hole and a supergiant, as functions of time. They showed that absolute and relative numbers of massive binary systems including neutron stars and black holes can serve as a good indicator of the age of the star formation burst. Popov et al. (1998) also made fits to dependencies $N(t)$ for different types of objects, where $N(t)$ is the number of sources, t is the time after the star formation burst.

Van Bever & Vanbeveren (2000) combined their close binary population number synthesis code with the formation mechanism of X-radiation in young supernova remnants and in high mass X-ray binaries. They demonstrated that the impact of interacting binaries is substantial.

Numerous point-like extragalactic X-ray sources were discovered during last years due to *Chandra* (see e.g. Muno et al. (2004), Grindlay et al. (2005)) and *XMM -Newton* (see e.g. Kong (2003), Georgakakis et al. (2004), Georgantopoulos et al. (2005)) missions. Some authors (Grimm et al. 2002, 2003; Gilfanov 2004; Kim & Fabbiano 2004) report about power law X-ray luminosity function:

$$\frac{dN}{dL} \sim L^{-\alpha} \times SFR, \alpha \approx 1.5, \qquad (3)$$

where SFR is the star formation rate.

These data were discussed by Postnov (2003) from theoretical point of view.

Grimm et al. (2003) realized that, within the accuracy of the presently available data, a linear relation between high mass X-ray binaries (HMXB) number and star formation rate (SFR) exists. They suggest that the relation between SFR and collective luminosity of HMXBs is nonlinear in the low-SFR regime, $L_x \sim SFR^{\sim 1.7}$, and becomes linear only for a sufficiently high star formation rate, $SFR \gtrsim 4.5 M_\odot$ yr^{-1} (for $M > 8 M_\odot$). Also they obtained the universal luminosity function of HMXBs and fitted the combined luminosity function of M82, Antennae, NGC 4579, 4736 and Circinus using a maximum-likelihood method with a power law with a cut-off at $L_c = 2.1 \cdot 10^{40}$ erg s^{-1} and normalized the result to the combined SFR of the galaxies. Their best-fitting luminosity function in the differential form is given by

$$\frac{dN}{dL_{38}} = (3.3^{+1.1}_{-0.8}) SFR \times L_{38}^{-1.61 \pm 0.12}, L < L_c, \qquad (4)$$

where $L_{38} = L/10^{38}$ erg s^{-1} and SFR is measured in units of $M_\odot$ per year.

Zezas et al. (2004) presented the X-ray luminosity function of the Antennae galaxies based on 8 observation performed with *Chandra*, 7 of them were obtained between January 2001 and November 2002. After combining all observations they detect a total of 120 sources down to a limiting luminosity of $\sim 2 \cdot 10^{37}$ erg s^{-1}. Authors suggested that comparison between the XLFs of the individual observations showed that they are not affected by source variability. The cumulative XLF of the coadded observations was represented by a single power law $N(> L) \sim L^{-0.52^{+0.08}_{-0.33}}$. There was an indication for a 'bump' at $\sim 10^{38}$ erg s^{-1}, but at this point its significance was not clear. If this bump is statistically significant it could be evidence for Eddington limited accretion on compact objects or anisotropic emission from the accretion disk (Zezas & Fabbiano 2002).

Belczynski et al. (2004) constructed synthetic X-ray binary populations for direct comparison with the X-ray luminosity function of NGC 1569 observed with *Chandra*. They produced hybrid models meant to represent the two stellar populations: one old and metal-poor, with continuous star formation for ~ 1.5 Gyr; and another a recent and metal-rich population. They found that for typical binary evolution parameters, it is possible to quite closely match the observed XLF shape.

Our critical points concerning both observational and theoretical aspects is in that that there is no observed universal luminosity function because:

1. Number of bright X-ray binaries is very small per galaxy.
2. We do not know real X-ray luminosity due to high variability of binary X-ray sources, on scales from seconds up to 100 years.

There is no simple (with one slope) theoretical universal luminosity function because:

1. X-ray population is the mix of different types of binaries with different mass exchange types.

2. Number of the systems with definite luminosity depends on spin evolution of a neutron star which has no direct connection to mass of its companion.

3. Theoretical arguments for universal function being at present time are not quite correct, because they exclude life-times (which depend on optical companion mass) of binary stars in accretion stage (Postnov 2003).

We stress that it is of great importance to take the spin evolution of NSs into account. Quantity of accreting neutron stars which give their contribution to the luminosity function is determined by their magnetic fields and spin periods. Neutron stars can be in a non-accreting state (propeller, ejector, see for details Lipunov (1992)). This circumstance usually is not taken into account in population synthesis models.

We must observe much more sources and determine their types to make correct luminosity function. In any case XLFs must have different slope for different types, ages and star formation histories in galaxies.

Ultra luminous X-ray sources (ULXs) with $L_x > 10^{39}$erg s^{-1} have been discovered in great amounts in external galaxies with *ROSAT*, *Chandra* and *XMM-Newton*. Rappaport et al. (2005) carried out a theoretical study to test whether a large fraction of the ULXs, especially those in galaxies with recent star formation activity, can be explained with binary systems containing stellar-mass BHs. To this end, they have applied a unique set of binary evolution models for BH X-ray binaries, coupled to a binary population synthesis code, to model the ULXs observed in external galaxies. They find that for donor stars with initial masses $\gtrsim 10M_\odot$ the mass transfer driven by the normal nuclear evolution of the donor star is sufficient to potentially power most ULXs. This is the case during core hydrogen burning and, to an even more pronounced degree, while the donor star ascends the giant branch, although the latter phases last only 5 per cent of the main-sequence phase. They show that with only a modest violation of the Eddington limit, e.g. a factor of 10, both the numbers and properties of the majority of the ULXs can be reproduced. One of their conclusions is that if stellar-mass BH binaries account for a significant fraction of ULXs in star-forming galaxies, then the rate of formation of such systems is $3 \cdot 10^{-7}$ yr^{-1} normalized to a core-collapse supernova rate of 0.01 yr^{-1}.

King et al. (2001) investigated models for the class of ultraluminous non-nuclear X-ray sources (ULXs) seen in a number of galaxies and probably associated with star-forming regions. The assumption of mild X-ray beaming suggests instead that ULXs may represent a short-lived but extremely common stage in the evolution of a wide class of X-ray binaries. The best candidate for this is the phase of thermal-timescale mass transfer that is inevitable in many intermediate- and high-mass X-ray binaries. This in turn suggests a link with the Galactic microquasars. The short lifetimes of high-mass X-ray binaries would explain the association of ULXs with episodes of star formation. These considerations still allow the possibility that individual ULXs may contain extremely massive black holes.

We also would like to remember the old consideration of the supercritical non-spherical accretion onto magnetized neutron stars (Lipunov 1982a,b). In this case matter falls to the magnetic poles of the neutron star. Maximum energy release proves to be $L = 46L_{Edd}(\mu_{30})^{4/9}$, where μ_{30} – is the magnetic dipole moment of the neutron star in 10^{30} G cm^3.

2. DESCRIPTION OF MODELS

2.1. Binaries under consideration and mechanisms of mass accretion

The "Scenario Machine" code includes the next types of the mass accretion by the compact star:

1. Accretion from the stellar wind.

2. Accretion from the disk-shaped stellar wind of Be-stars.

3. Mass transfer through the inner Lagrange point during Roche lobe overflow stage:

   (a) On thermal timescale.

   (b) On nuclear timescale.

   (c) On magnetic stellar wind timescale.

   (d) On gravitational radiation timescale.

Induced stellar wind is not included into the program.

Most of the X-ray pulsars in the Milky Way belong to binaries which consist of the Be-star and the neutron star (Liu et al. 2000; Lij et al. 2001; Raguzova & Popov 2005). The mass loss by the Be-star is determined by its rotation. Its mass influences onto its wind to a lesser degree. At the same time we see a little part of the X-ray binaries consisting of Be- and neutron stars due to variability of mass transfer processes and the transient character of accretion in such systems (van den Heuvel 1994).

So, we should study as much types of X-ray binaries as possible. This is the list of the systems under our consideration:

1. NA+I: the accreting neutron star with the main sequence companion.
2. NA+II: the accreting neutron star with the super giant companion.
3. NA+III: the accreting neutron star with the companion filling its Roche lobe.
4. NA+Be: the accreting neutron star with the Be-star companion.
5. BH+II: the black hole with the super giant companion.
6. BH+III: the black hole with the companion filling its Roche lobe.
7. SNA+III: the super accreting neutron star with the companion filling its Roche lobe.
8. SBH+III: the super accreting black hole with the companion filling its Roche lobe.

The last two types of systems are taken into consideration for the purpose of modelling of ULXs. Radiation of such objects can be strongly collimated (see e.g. Cherepashchuk et al. (2005)) to a degree $\sim 1^\circ$. Also we take into account possibility of mild beaming (see e.g. King et al. (2001)). If the radiation of the source is collimated, then we should reduce calculated number of binaries using formula

$$N_o = \frac{\Omega}{4\pi} N_c, \qquad (5)$$

because we can not see the object if its beam is directed away from us. We recalculate X-ray luminosity of such systems using formula

$$L_o = \frac{4\pi}{\Omega} L_c, \qquad (6)$$

in order to obtain the luminosity under the formal assumption of spherically symmetric radiation. In these equations Ω is the doubled solid collimation angle of the radiation, L_c is the calculated luminosity of the source and N_c is the calculated number of sources, L_o and N_o are the same observable values.

We have to say some words about Wolf-Rayet (WR) stars with black holes or neutron stars. Number of binaries consisting of the accreting black hole and the WR-star is very small, because WR-stars have very high velocity of the wind. That is why accretion disks are not able to form in wide pairs (with orbital period $\gtrsim 10$ hours; orbital period of Cyg X-3, for example, is ≈ 5 hours; see for detailed description Karpov & Lipunov (2001)). There are no binaries consisting of WR-stars and accreting NSs, because NSs accelerate their rotation during second mass exchange (recycling) and therefore become propellers or ejectors (Lipunov 1982c) in such kind of binaries.

Note that our conclusions concerning accreting neutron stars with Be-stars, super accreting neutron stars with non-degenerate stars filling their Roche lobes, super accreting black holes with non-degenerate stars filling their Roche lobes have approximate character, because it is impossible to depict correctly temporal and angular dependencies of their radiation at present time. Our calculations show that real luminosity function is compound.

2.2. List of main evolutionary parameters

Since the algorithms used in the "Scenario Machine" have been described many times, we shall only note the most important evolutionary parameters influencing the results of the numerical modeling of the binaries under consideration. A detailed description of the "Scenario Machine" can be found in the next works: Lipunov et al. (1996b,c, 2007).

The initial masses of primary components were varied between $10M_\odot$ and $120M_\odot$. To describe

also a kind of ULX objects consisting of a black hole with mass higher than $\sim 100M_\odot$ and an optical star in Roche lobe overflow stage we have conducted a population synthesis also with lower and upper limits equal to $120M_\odot$ and $1000M_\odot$ correspondingly.

We assume zero initial eccentricity, all initial mass ratios have equal probability, initial mass of the secondary star is in the range $0.1M_\odot$ – mass of the primary star.

Mass loss by optical stars in the course of their evolution remains incompletely explored. Despite the fact that is has been possible to substantially reduce the uncertainties (see, e.g., (Bogomazov et al. 2005)), no clear justification for a choice of a standard scenario has emerged. Therefore, we carried out our computations for two scenarios for mass loss by non-degenerate stars, which we call A and C. A detailed description of these models can be found in (Lipunov et al. 2007). Scenario A has a weak stellar wind. The stellar wind of massive stars (with masses higher than $15M_\odot$) is higher in scenario C, for lower-mass stars, scenarios A and C are equivalent. The total mass loss in any evolutionary stage is higher in scenario C than in scenario A.

Common envelope stage efficiency α_{CE} is equal to 0.5.

Minimal initial mass of the star which produces a black hole as the result of its evolution is $25M_\odot$. We assume the parameter $k_{bh} = M_{bh}/M_{PreSN}$ to be equal to 0.5 (see Bogomazov et al. (2005) for detailes), M_{PreSN} is the mass of the pre-supernova star which produced the black hole with mass M_{bh}.

Initial mass of the new-born neutron star is randomly distributed in the range 1.25 – $1.44M_\odot$. Maximum mass of the NS (Oppenheimer-Volkoff limit) equals to $M_{OV} = 2.0M_\odot$ in our calculations. Initial value of the magnetic field of NSs is assumed to be equal to 10^{12} Gs, the field decay time is assumed to be equal to 10^8 years. Characteristic kick velocity of the new-born neutron star we accept to be equal to 80 km s^{-1} in this work.

We use two different values of collimation angle for supercritical regimes of accretion: $\alpha = 1^\circ$ and $\alpha = 10^\circ$.

2.3. Result normalization

Birth frequencies of binaries were calculated using the next formula:

$$\nu_{gal} = \frac{N_{calc}}{N_{tr}} \frac{1}{M_1^{1.35}}, \quad (7)$$

here ν_{gal} is the frequency of birth of a specific binary system type in a spiral galaxy, N_{calc} is the number of the systems under our consideration appeared during calculations, N_{tr} is the total number of binaries which evolution was calculated, M_1 is the minimal initial mass of a star in our calculations. We treat a spiral galaxy in this case as a galaxy with constant star formation rate which is defined by the Salpeter function.

Quantities of the systems in a spiral galaxy were calculated using equation (8).

$$N_{gal} = \frac{\sum t_i}{N_{tr}} \frac{1}{M_1^{1.35}}, \quad (8)$$

here N_{gal} is the quantity of a specific binary system type in a spiral galaxy, t_i is the life time of the binary system under consideration.

Along with modeling population in the spiral galaxy we also made some estimations of evolution of X-ray luminosity function and total X-ray luminosity in an elliptical galaxy. Quantities of the systems in the elliptical galaxy were calculated using equation (9).

$$N_{gal} = N_{calc} \frac{M_{gal}}{M_{ScM}} \left(\frac{M_{1ScM}}{M_{1gal}} \right)^{-1.35} \frac{\sum t_i}{\Delta T}, \quad (9)$$

here $M_{gal} = 10^{11} M_\odot$ is the mass of typical galaxy, M_{1ScM} is the minimal initial mass of a star in our calculations, $M_{1gal} = 0.1M_\odot$ is the minimal initial mass of a star, t_i is the life time of a binary system under our consideration in the range of the time interval between T and $T + \Delta T$. We treat an elliptical galaxy in this work as a kind of object in which all stars born at the same time and then evolve (δ-function star formation rate).

2.4. Constraints on key parameters of the evolutionary scenario

Previous estimates of the ranges of parameters determining the evolution of binaries were obtained by Lipunov et al. (1996c, 1997).

Since that time, some new results related to the evolution of binaries have been obtained, and we carried out additional computations of constraints that can be applied to the parameters of the evolutionary scenario. The latest observational estimates of the kick velocities received by NSs in supernovae explosions are given by Hobbs et al. (2005), where it is concluded that the typical kick magnitude is $\sigma = 265$ km s^{-1}.

An attempt to obtain a more accurate estimate of the mass-loss efficiency in the common-envelope stage was made by Dewi & Tauris (2000), who tried to take into account the concentration of the stellar material toward the center: $\frac{GM_d(M_d-M_c)}{R_d\lambda}$. However, they assumed that the efficiency in the common-envelope stage was $\mu_{CE} = 1$. In general, this parameter is not known accurately. Our coefficient α_{CE} is the product of μ_{CE} and the parameter λ considered by Dewi & Tauris (2000), which describes the concentration of the stellar matter toward the center. For this reason, we use the value of α_{CE} suggested by Lipunov et al. (1996c).

We would like to note one more important circumstance. Ill-defined parameters of the evolutionary scenario, such as v_0, α_{CE}, the stellar wind efficiency, and so on, are internal parameters of the population synthesis. In the future, they may be defined more precisely, or their physical meaning may change: the kick-velocity distribution may turn out not to be Maxwellian, it may be that the complex hydrodynamics of common envelopes cannot be described using the parameters α_{ce} and λ, the mass ratio distribution $f(q)$ may be not a power law. There exists only one way to verify our results: comparison of our model predictions with observational data.

For this reason, we suggest two quantities to be compared to test the model: the ratio of the calculated and observed numbers of Cyg X-3 systems, and the ratio of the number of binary radio pulsars with NS companions and the total number of radio pulsars (both single and binary), $\frac{N_{Psr+NS}}{N_{Psr}}$, where N_{Psr+NS} is the number of radio pulsar in binary systems with a neutron star, N_{Psr} is the total number of radio pulsars, binary and single. To avoid the need to differentiate between young pulsars and old pulsars that have been accelerated by accretion, we consider only young pulsars. Note that the observed value of this ratio is ~ 0.001 (ATNF catalogue 2006): among more than 1500 known single and binary radio pulsars, only two young pulsars in pairs with NSs have been discovered (J2305+4707 and J0737-3039). As a model of a Cyg X-3 type system, we take a binary containing a BH with WR companion that is more massive than $> 7M_\odot$ and having an orbital period 10 hours.

Figure 3 of the calculated number of binaries with a NS and radio pulsar N_{Psr+NS} and the calculated sum of the numbers of single and binary radio pulsars N_{psr} depends on the kick velocity v_0. The width of the shaded region reflects the variation of the efficiency of the common envelope stage α_{CE} in the range 0.21.0.

Figure 3 shows the OCCO criterion (Lipunov et al. 1996b) for the ratio $\frac{N_{Psr+NS}}{N_{Psr}}$. The typical kick velocity v_0 is plotted along the horizontal axis. The width of the shaded region reflects the variation of the efficiency of the common envelope stage α_{CE} in the range 0.21.0. The observed value of $\frac{N_{Psr+NS}}{N_{Psr}}$ is ~ 0.001.

As seen from Figs. 3 and 3, the characteristic value of kick velocity v_0 cannot exceed ≈ 200 km s^{-1}. By this reason we make use of the results of paper (Lipunov et al. 1997).

Figure 3 shows the number of Galactic Cyg X-3 systems in our model as a function of the common envelope efficiency. This figure shows that we can essentially exclude values $\alpha_{CE} < 0.3$.

3. RESULTS AND CONCLUSIONS

Four simulations runs were performed, each simulating the evolution of $1 \cdot 10^7$ binary systems. Two of them were performed with weak stellar wind (stellar wind type A), and other models with reasonably high stellar wind (stellar wind type C). In each of these cases we made our calculations using two value areas of initial mass of the primary star in Salpeter's power law: in the range $10 - 120M_\odot$ for investigations of all types of systems under consideration, and in the range $120-1000M_\odot$ to qualitatively depict only ultra luminous objects consisting of super accreting intermediate mass black holes with companions filling their Roche lobes.

In the Figures 3 and 5 we show birth frequency of different types of X-ray sources in the spiral galaxy. In the Figures 3 and 7 we present cumulative luminosity functions of different types of

X-ray sources in the same galaxy. Figures 3 and 3 were calculated using stellar wind type A (weak stellar wind). Figures 5 and 7 were calculated using stellar wind type C (moderate stellar wind). Marks in Figures 4 – 7 are (see abbreviation in Section 2.1) : 1, NA+I; 2, NA+II; 3, NA+III; 4, NA+Be; 5, BH+II; 6, BH+III; 7a, SNA+III, collimation angle (for super critical regimes of accretion) $\alpha = 10°$; 7b, SNA+III, $\alpha = 1°$; 8a, SBH+III, $\alpha = 10°$; 8b, SBH+III, $\alpha = 1°$; 9a, SBH+III, $\alpha = 10°$; 9b, $\alpha = 1°$. For curves 9a, 9b minimal initial mass of the primary star is $120M_{\odot}$, in other cases it is equal to $10M_{\odot}$.

As one can see from Figures 3 – 7, different types of X-ray binary systems belong to different luminosity ranges, their luminosity functions have different slope. These facts are evidence of complexity of the X-ray luminosity function.

Comparisons between figures 4 and 5, 6 and 7 convince us of the importance of taking into account life times of X-ray stages in theoretical models of XLFs. Relative abundances of different types of X-ray binary systems in the birth frequency function and in the luminosity function are different. For example, we can see from Figure 4 that the birth frequency of NA+II X-ray binaries is about ten times higher than the birth frequency of NA+I X-ray binaries. But the super giant life time is much shorter than the life time of the main sequence star, so, as we can see from Figure 5, quantity of NA+I binaries is only two times less than quantity of NA+II systems in the spiral galaxy. Stronger stellar wind (type C) makes this difference even greater (compare Figures 6 and 7).

The stellar wind magnitude essentially influences the scenario for two reasons. First, the spherically symmetric wind leads to increase in component separation. Secondly, stellar wind greatly affects the final evolutionary outcome of massive stars. In particular, the choice of wind strength will change the mass distribution of black holes seen in the population (Bogomazov et al. 2005), as the black hole progenitor loses a different amount of mass prior to collapse. Moreover, the total mass loss of a star by wind may cause a change in its remnant type (it may produce a neutron star instead of a black hole). We can see from Figures 4 – 7 that stronger stellar wind (type C) dramatically decreases quantities of many types of X-ray binaries (and affects all kind of them).

In the Figures 8 and 9 we show cumulative luminosity functions of all investigated systems in the spiral galaxy like the Milky Way. See Tables 1 and 2 for numerical data. In these Figures α is the collimation angle in supercritical regimes of accretion. Figure 8 was calculated under the assumption of stellar wind type A, Figure 9 was calculated under the assumption of stellar wind type C.

Figures 8 and 9 show that the X-ray luminosity function has different slope in different ranges of luminosity (see also Tables 1 and 2 for numerical data). Grimm et al. (2002) argued that the best values of the slope and normalization of the cumulative form of the luminosity function is

$$N(>L) = 5.4 \times SFR \left(L^{-0.61 \pm 0.12} - 210^{-0.61 \pm 0.12} \right); \quad (10)$$

over the luminosity range between $\sim 10^{35}$ erg s^{-1} and $\sim 10^{40}$ erg s^{-1} (see Figure 5 and Equation 7 in their paper, but they gave narrower luminosity range as the result in Conclusions of the article). Our calculations show similar XLF slope over the ranges between $\approx 2 \cdot 10^{37}$ erg s^{-1} and $\approx 10^{38}$ erg s^{-1}, and between $\approx 2 \cdot 10^{39}$ erg s^{-1} and $\approx 10^{41}$ erg s^{-1} (the last range depends on our assumptions about the collimation angle of the X-ray emission in cases of super critical accretion). Between these two ranges the XLFs (our theoretical curves) become very steep due to Eddington limit (there are a lot of NA+III systems, and their luminosity is about this value, see Figures 3 – 7).

In the Figures 10 and 11 we show birth frequency (a) of all investigated systems (differential function) and differential luminosity function (b) of X-ray binary sources in the Galaxy. Marks in the Figures are: 1, collimation angle (for super critical regimes) $\alpha = 10°$; 2, $\alpha = 1°$. Figure 10 was calculated under the assumption of stellar wind type A, Figure 11 was calculated under the assumption of stellar wind type C. Luminosity functions in differential form also have different slope, there is no evidence for the universal XLF.

In the Figure 12 we show cumulative luminosity functions of all investigated systems in the elliptical galaxy after the star formation burst. The curves in the Figure represent the next models: 1, stellar wind type A, collimation angle (for super critical regimes) $\alpha = 10°$; 2, wind A, $\alpha = 1°$;

3, wind C, $\alpha = 10°$; 4, wind C, $\alpha = 1°$. The time ranges after the star formation burst in the Figure are: a, 0-10 million years; b, 10-100 million years; c, 100 million – 1 billion years; d, 1-10 billion years. v Figure 12 shows the evolution of luminosity function on a long timescale after the stellar formation burst in the elliptical [2] galaxy. As one can see from this Figure, there is no evidence for the universal XLF. Nevertheless, note that numbers of systems in this figure are quite relative. Any systems were added to the number of the systems in appropriate interval of time if they born as X-ray system or still show itself as X-ray source during this period or part of it, but life time of a system can be less than the duration of the period and a system can born not in the beginning of the period. For more precision it is necessary to take less intervals of time, but our purpose is to show long time evolution qualitatively.

Belczynski et al. (2004) found that the dependence of the XLF slope on age is non-monotonic in the dwarf (post)starburst galaxy NGC 1569. They studied behavior with time of theoretical normalized XLFs for two stellar populations: one old at 1.5 Gyr and one young at age 10, 70, and 170 Myr (continuous SFR through 1.5 Gyr, and 10, 70, and 100 Myr, respectively). The average SFR in the old population was assumed to be 20 times smaller than that in the young population. Direct comparison between our results is difficult, because we use different star formation models in our calculations. One of the common features is in that that the XLF should evolve with time. Also we suggest that their XLFs can be fitted by broken power laws, Belczynski et al. (2004) did not obtain uniform XLF in NGC 1569.

In the Figure 13 we show the evolution of the X-ray luminosity after the star formation burst ($T = 0$) in the galaxy with mass $10^{11} M_{\odot}$. See Table 2 for numerical data. In this Figure: 1, our calculations, stellar wind type A; 2, the result obtained by Tatarinzeva et al. (1989); 3, our calculations, stellar wind type C. We should note that in comparison with results obtained by Van Bever & Vanbeveren (2000) we do not take into account the X-ray emission from supernova remnants in our models. Our data in this Figure start at their end point (10 Myr). After $4 \cdot 10^2$ million years since star formation burst in the galaxy its X-ray luminosity can be rather well fitted by power law $L(T) \sim T^{-a}$; a is equal to 1.56 and 1.8 in very wide range of time (see Table 3 for details). Previous work (Tatarinzeva et al. 1989) showed approximately the same result which we can confirm. The cause of differences is in that that 16 years ago calculations were conducted if authors were taking into consideration not so much types of systems as in the present work. Also models of evolution of binaries have changed. Stronger stellar wind (see Table 4) makes the our result almost inconsistent with Tatarinzeva et al. (1989).

So, our calculations show the next results:

1. X-ray luminosity function of binary X-ray sources is complicated, it has different slope in different ranges of luminosity. So, there is no universal X-ray luminosity function of binary X-ray sources.

2. X-ray luminosity function of binary X-ray sources depends on the star formation rate as it was first shown in 1989 (Tatarinzeva et al. 1989).

3. It is necessarily to take into account spin evolution of neutron stars and life times of all stages during theoretical modelling of X-ray luminosity function of binary X-ray sources.

[2] In this work we treat the galaxy as "elliptical" if the object has mass $10^{11} M_{\odot}$ and δ-function starburst.

REFERENCES

Abt, H. A. 1983, ARA&A, 21, 343

Manchester, R. N., Hobbs, G. B., Teoh, A. & Hobbs, M. 2005 (1993-2006), AJ, 129 (the Australia Telescope National Facility (ATNF) pulsar catalogue, avialable at: http://www.atnf.csiro.au/research/pulsar/psrcat/)

Belczynski, K., Kalogera, V., Zezas, A., & Fabbiano, G. 2004, ApJ, 601, 147

Bogomazov, A. I., Abubekerov M. K., Lipunov, V. M.2005, Astronomy Reports, 49, 644

Dewi, J. D. M., & Tauris, T. M. 2000, A&A, 360, 1043

Georgantopoulos, I., Georgakakis, A., & Koulouridis, E. 2005, MNRAS, 360, 782

Gilfanov, M. 2004, MNRAS, 349, 146

Grimm, H.-J., Gilfanov, M., & Sunyaev, R. 2002, A&A, 391, 923

Grimm, H.-J., Gilfanov, M., & Sunyaev, R. 2003, MNRAS, 339, 793

Hobbs, G., Lorimer, D. R., Lyne, A. G., & Kramer, M. 2005, MNRAS, 360, 974

Karpov, S. V., & Lipunov, V. M. 2001, Astron. Letters, 2001, 27, 10, 645-647

Kim, D.-W., & Fabbiano, G. 2004, ApJ, 611, 846

King, A. R., Davies, M. B., Ward, M. J., Fabbiano, G. & Elvis, M. 2001, ApJ, 552, L109

Kong, A. K. H. 2003, MNRAS, 346, 265

Lipunov, V. M. 1982a, Ap&SS, 82, 343

Lipunov, V. M. 1982b, SvA, 26, 54

Lipunov, V. M. 1982c, SvAL, 8, 194

Lipunov, V. M. 1992, Astrophysics of Neutron Stars, Springer-Verlag, Berlin - Heidelberg - New York, Astronomy and Astrophysics Library, 322

Lipunov, V. M., Ozernoy, L. M., Popov, S. B., Postnov, K. A., & Prokhorov, M. E. 1996a, ApJ, 466, 234

Lipunov, V. M., Postnov, K. A., & Prokhorov, M. E. 1996b, ed. R. A. Sunyaev, The Scenario Machine: Binary Star Population Synthesis, Astrophysics and Space Physics Reviews, vol. 9, Harwood academic publishers

Lipunov, V. M., Postnov, K. A., & Prokhorov, M. E. 1996, A&A, 310, 489

Lipunov, V. M., Postnov, K. A., & Prokhorov, M. E., 1997, MNRAS, 288, 245

Lipunov, V. M. 2006, IAU proseedings, Populations of High Energy Sources in Galaxies Proceedings of the 230th Symposium of the International Astronomical Union, Edited by E. J. A. Meurs, G. Fabbiano, Cambridge University Press, 2006, p. 391

Lipunov, V. M., Postnov, K. A., Prokhorov, M. E., Bogomazov A. I. 2007, arXiv:0704.1387v1

Liu, Q. Z., van Paradijs, J., & van den Heuvel, E. P. J. 2000, A&A, 147, 25

Liu, Q. Z., van Paradijs, J., & van den Heuvel, E. P. J. 2000, A&A, 368, 1021

Muno, M. P. 2004, ApJ, 613, 1179

Popov, S. B., Lipunov, V. M., Prokhorov, M. E., & Postnov, K. A. 1998, Astronomy Reports, v. 42, p. 29

Postnov, K. A. 2003, Astron. Lett., 29, 372

Raguzova, N. V., & Popov S. B. 2005 Astronomical and Astrophysical Transactions, 24, 151

Rappaport, S. A., Podsiadlowski, Ph., & Pfahl, E. 2005, MNRAS, 356, 401

Tatarintzeva, V., Lipunov, V., Osminkin, E., & Prokhorov M. E. 1989, In ESA, The 23rd ESLAB Symposium on Two Topics in X-Ray Astronomy, v.1: X Ray Binaries, p. 653

Van Bever, J., & Vanbeveren, D. 2000, A&A, 358, 462

van den Heuvel, E. P. J. 1994, in Shore S.N., Livio M., van den Heuvel E.P.J., Interacting Binaries, Springer-Verlag, p. 103

Zezas, A., & Fabbiano, G. 2002, ApJ, 577, 726

Zezas, A., Fabbiano, G., Baldi, A., King, A. R., Ponman, T. J., Raymond, J. C., & Schweizer, F. 2004, RevMexAA, 20, 53

Cherepashchuk, A. M., et al. 2005, A&A, 437, 561

Georgakakis, A., et al. 2004, MNRAS, 349, 135

Grindlay, J. E., et al. 2005, ApJ, 635, 920

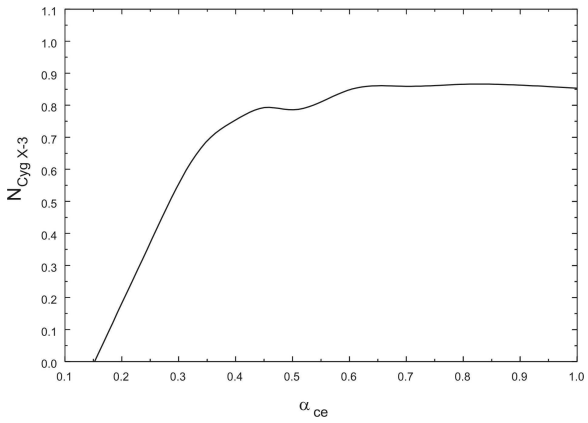

Fig. 1.— Calculated number of Cyg X-3 type systems in the Galaxy as the function of the common envelope stage efficiency α_{CE}.

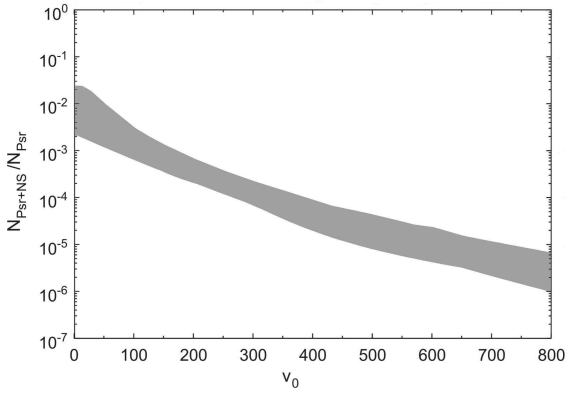

Fig. 2.— This figure shows how the ratio $\frac{N_{Psr+NS}}{N_{Psr}}$ depends on the kick velocity v_0. Here N_{Psr+NS} is the calculated number of binary neutron stars with radio pulsars and N_{Psr} is the calculated number of all radio pulsars, binary and single. "Width" of the filled area depicts various values of α_{CE} in the range $0.2 - 1.0$.

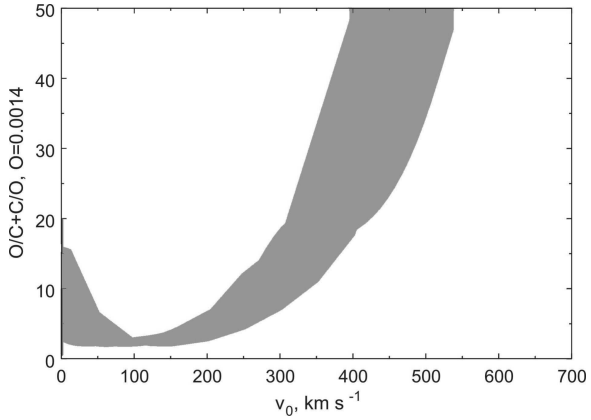

Fig. 3.— This figure shows OCCO criterion (Lipunov et al. 1996b) for the ratio $\frac{N_{Psr+NS}}{N_{Psr}}$, v_0 is the characteristic kick velocity. "Width" of the filled area depicts various values of α_{CE} in the range between 0.2 and 1.0. Observational value of the ratio $\frac{N_{Psr+NS}}{N_{Psr}}$ is ~ 0.001.

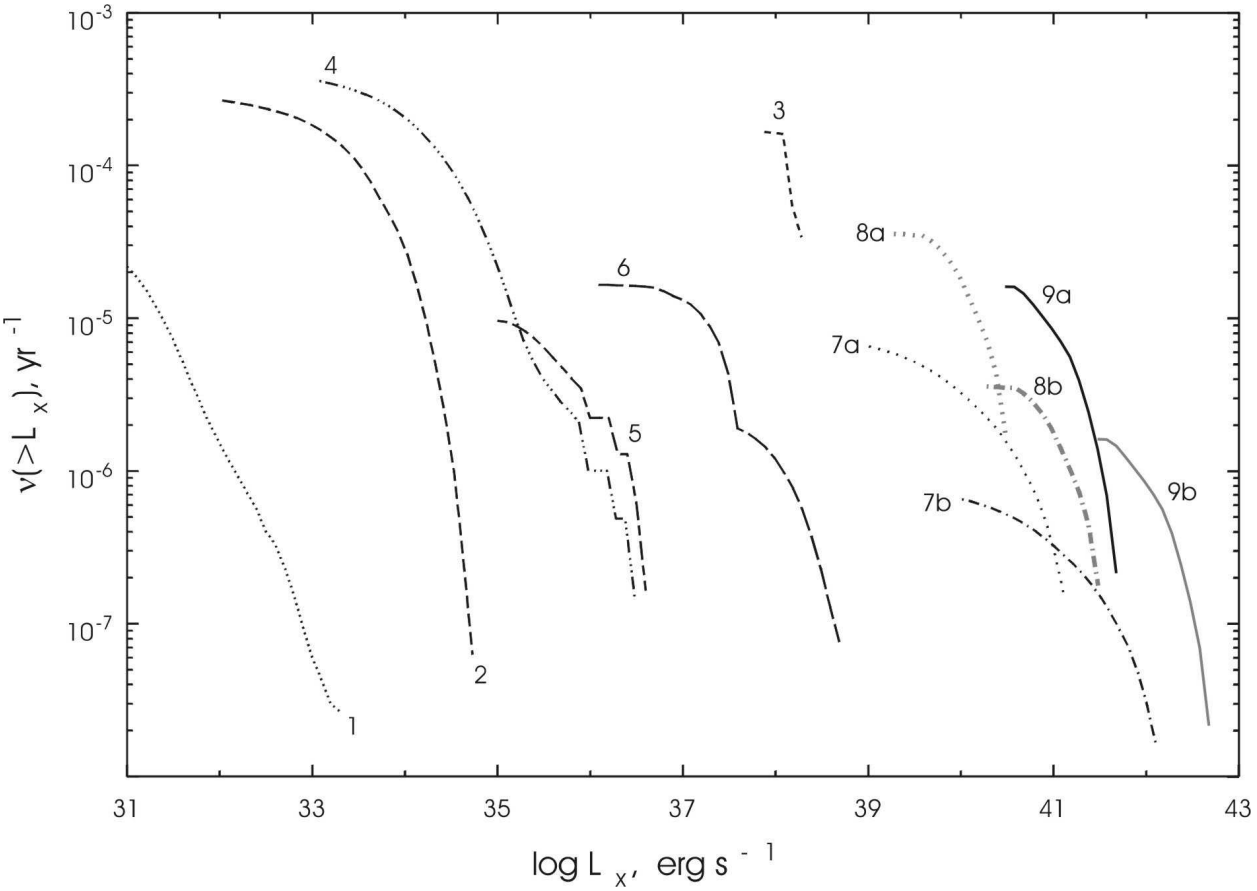

Fig. 4.— Birth frequency for different types of X-ray sources in the Galaxy. Marks in the Figure are: 1, NA+I; 2, NA+II; 3, NA+III; 4, NA+Be; 5, BH+II; 6, BH+III; 7a, SNA+III, collimation angle $\alpha = 10°$; 7b, SNA+III, $\alpha = 1°$; 8a, SBH+III, $\alpha = 10°$; 8b, SBH+III, $\alpha = 1°$; 9a, SBH+III, $\alpha = 10°$; 9b, $\alpha = 1°$. For curves 9a, 9b minimal initial mass of the primary star is $120M_\odot$, in other cases it is equal to $10M_\odot$. These calculations were conducted using stellar wind type A.

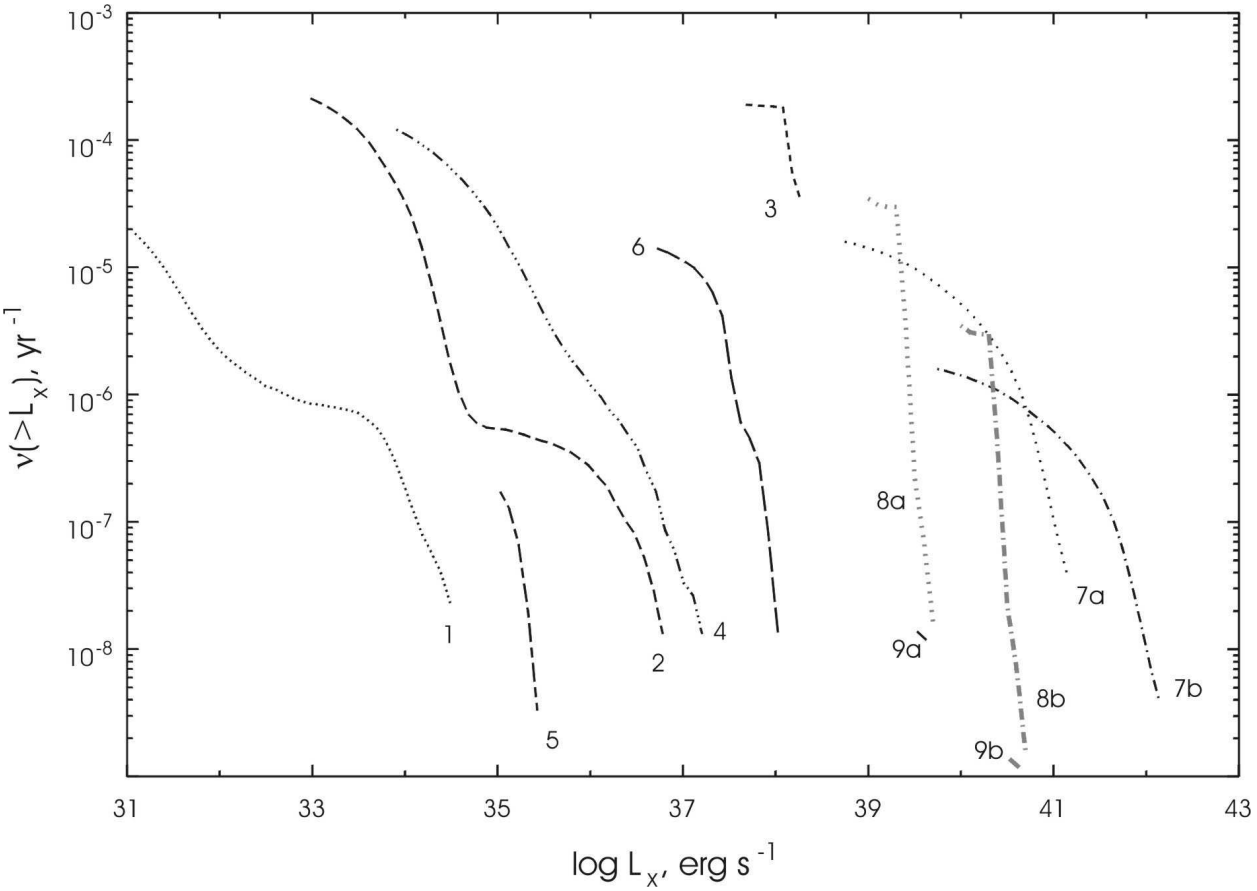

Fig. 5.— Birth frequency for different types of X-ray sources in the Galaxy. Marks in the Figure are: 1, NA+I; 2, NA+II; 3, NA+III; 4, NA+Be; 5, BH+II; 6, BH+III, 7a, SNA+III, collimation angle $\alpha = 10°$; 7b, SNA+III, $\alpha = 1°$; 8a, SBH+III, $\alpha = 10°$; 8b, SBH+III, $\alpha = 1°$; 9a, SBH+III, $\alpha = 10°$; 9b, $\alpha = 1°$. For curves 9a, 9b minimal initial mass of the primary star is $120M_\odot$, in other cases it is equal to $10M_\odot$. These calculations were conducted using stellar wind type C.

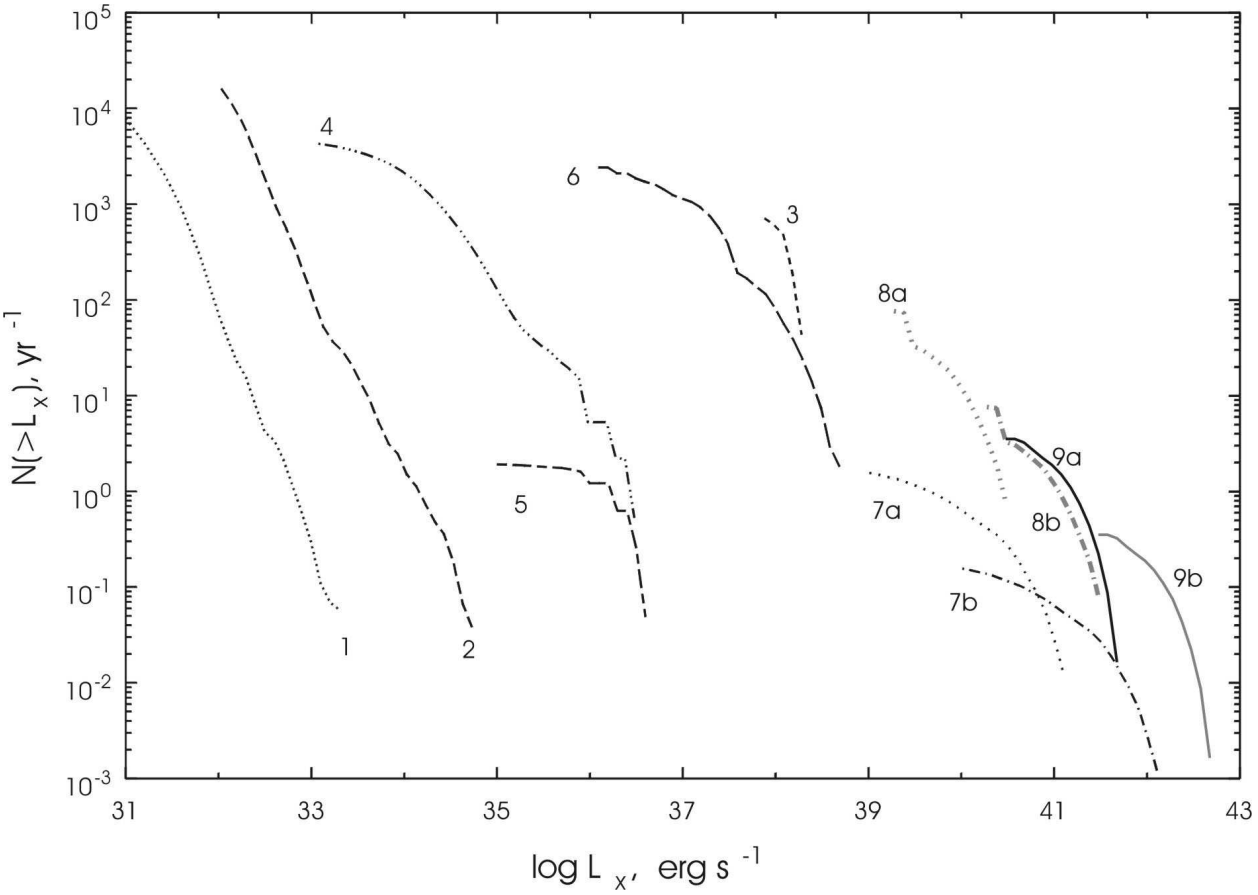

Fig. 6.— Cumulative luminosity functions of different types of X-ray sources in the Galaxy. Marks in the Figure are: 1, NA+I; 2, NA+II; 3, NA+III; 4, NA+Be; 5, BH+II; 6, BH+III; 7a, SNA+III, collimation angle $\alpha = 10°$; 7b, SNA+III, $\alpha = 1°$; 8a, SBH+III, $\alpha = 10°$; 8b, SBH+III, $\alpha = 1°$; 9a, SBH+III, $\alpha = 10°$; 9b, $\alpha = 1°$. For curves 9a, 9b minimal initial mass of the primary star is $120M_\odot$, in other cases it is equal to $10M_\odot$. These calculations were conducted using stellar wind type A.

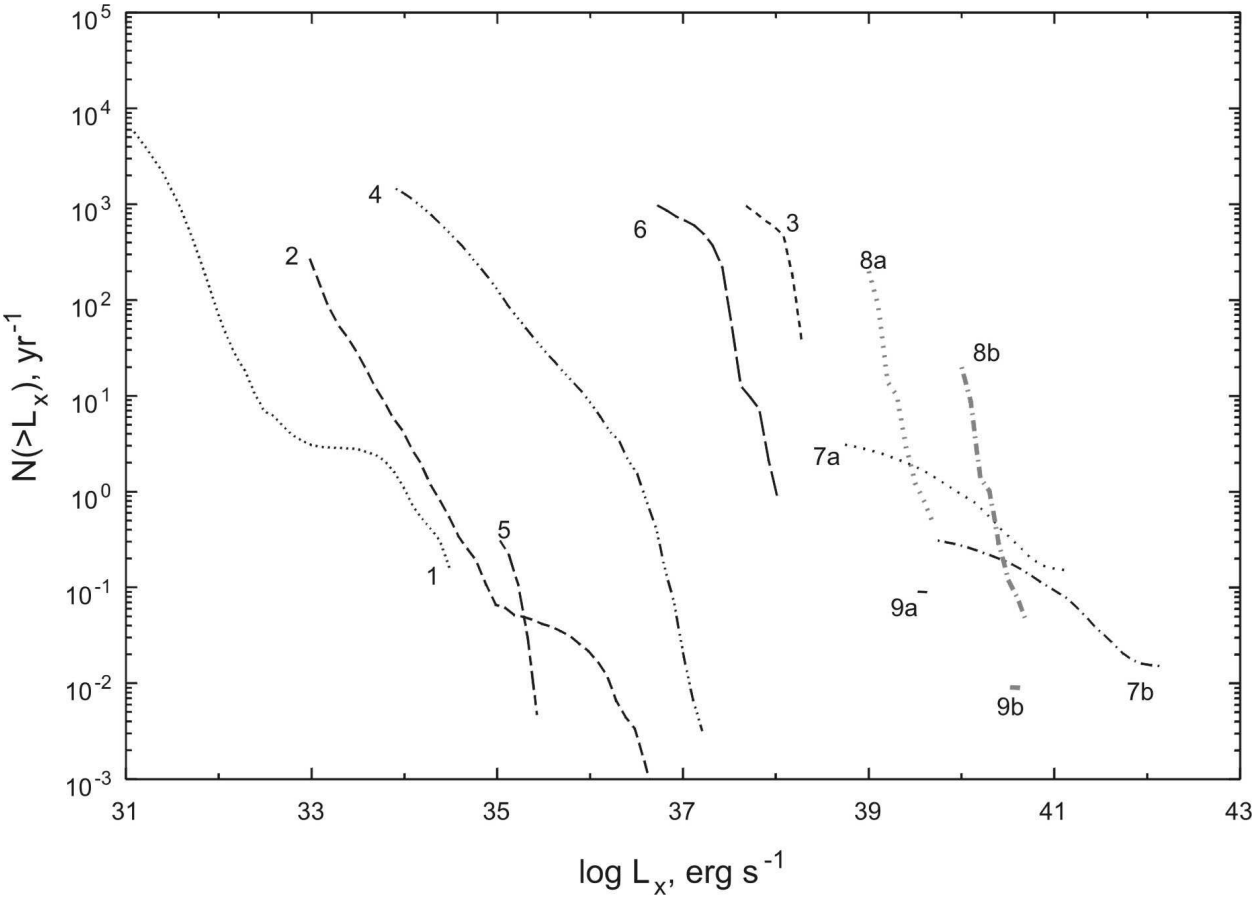

Fig. 7.— Cumulative luminosity functions of different types of X-ray sources in the Galaxy. Marks in the Figure are: 1, NA+I; 2, NA+II; 3, NA+III; 4, NA+Be; 5, BH+II; 6, BH+III, 7a, SNA+III, collimation angle $\alpha = 10°$; 7b, SNA+III, $\alpha = 1°$; 8a, SBH+III, $\alpha = 10°$; 8b, SBH+III, $\alpha = 1°$; 9a, SBH+III, $\alpha = 10°$; 9b, $\alpha = 1°$. For curves 9a, 9b minimal initial mass of the primary star is $120M_\odot$, in other cases it is equal to $10M_\odot$. These calculations were conducted using stellar wind type C.

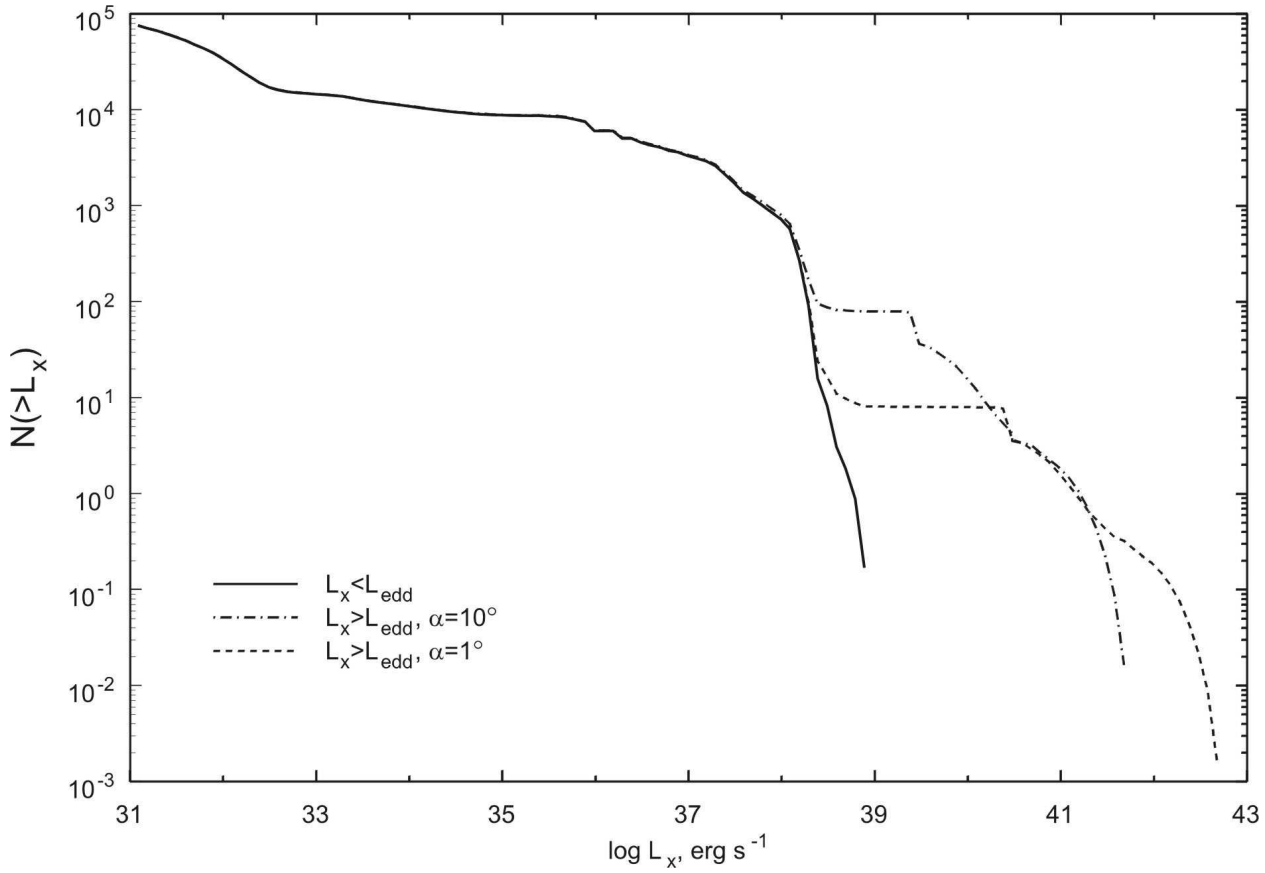

Fig. 8.— Cumulative luminosity functions of all investigated systems in the galaxy like the Milky Way. See Table 1 for numerical data. In this Figure α is the collimation angle in supercritical regimes of accretion. These calculations were conducted using stellar wind type A.

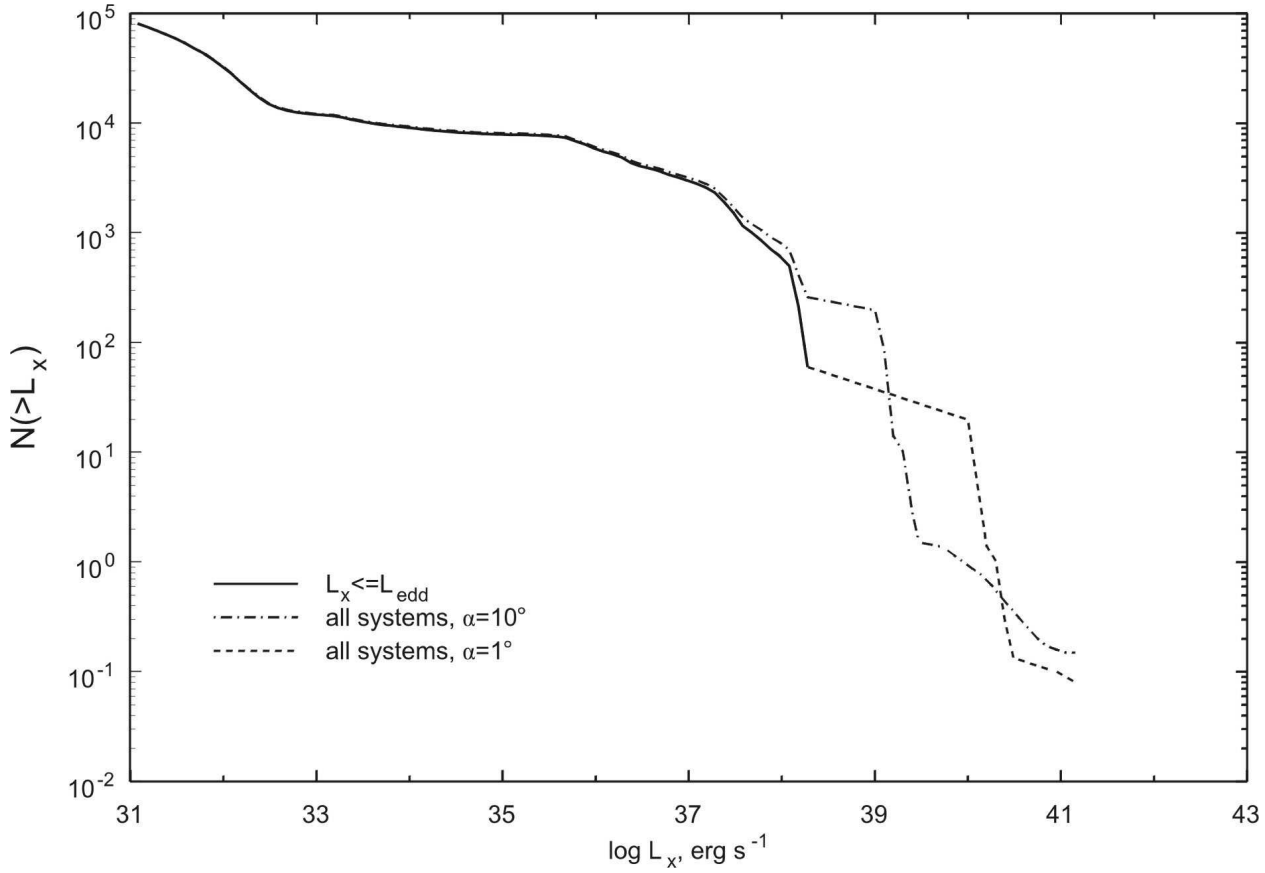

Fig. 9.— Cumulative luminosity functions of all investigated systems in the galaxy like the Milky Way. See Table 1 for numerical data. In this Figure α is the collimation angle in supercritical regimes of accretion. These calculations were conducted using stellar wind type C.

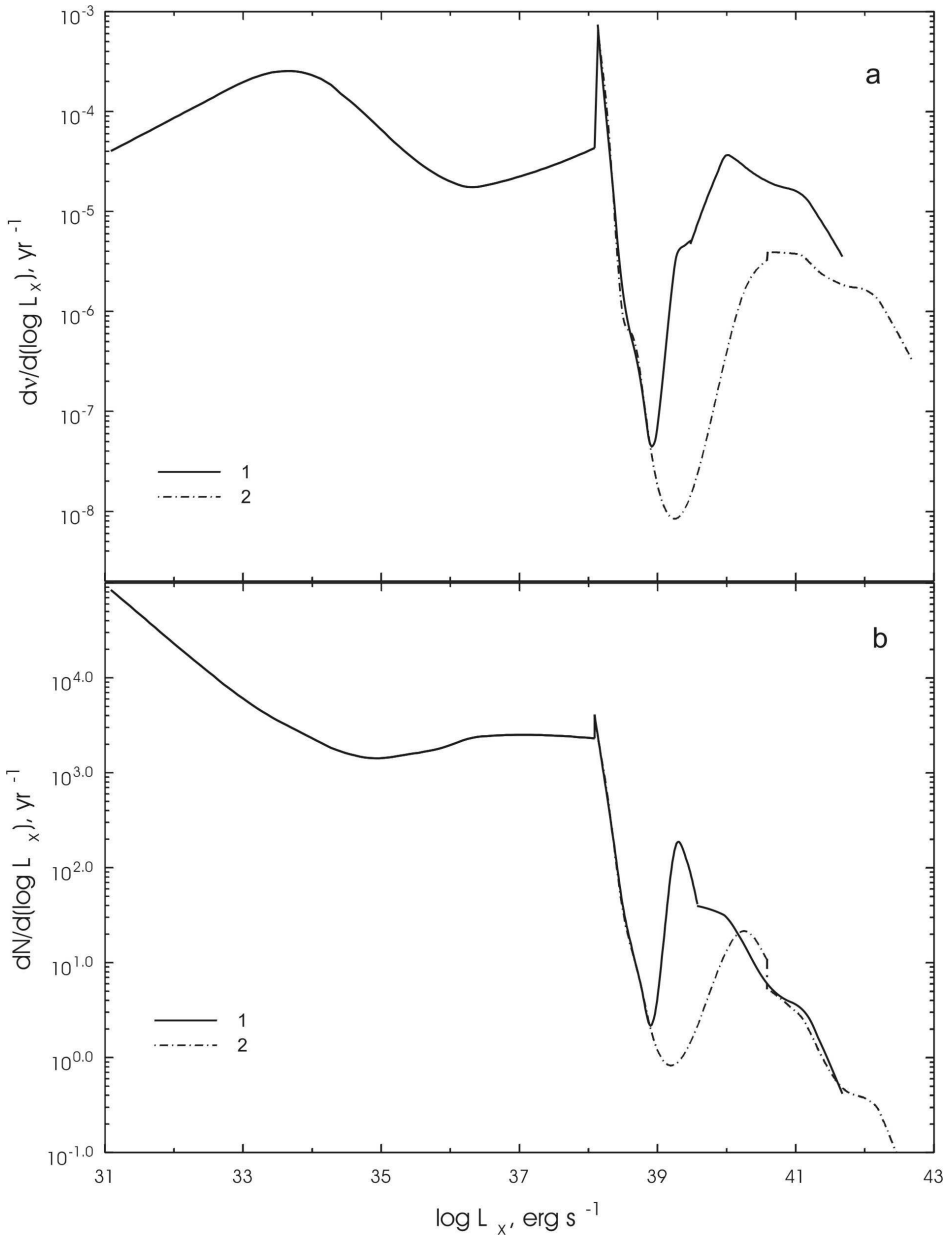

Fig. 10.— Birth frequency (a) of all investigated systems (differential function) and differential luminosity function (b) of X-ray binary sources in the Galaxy. Stellar wind type A. Marks in the Figure are: 1, collimation angle (for super critical regimes) $\alpha = 10°$; 2, $\alpha = 1°$.

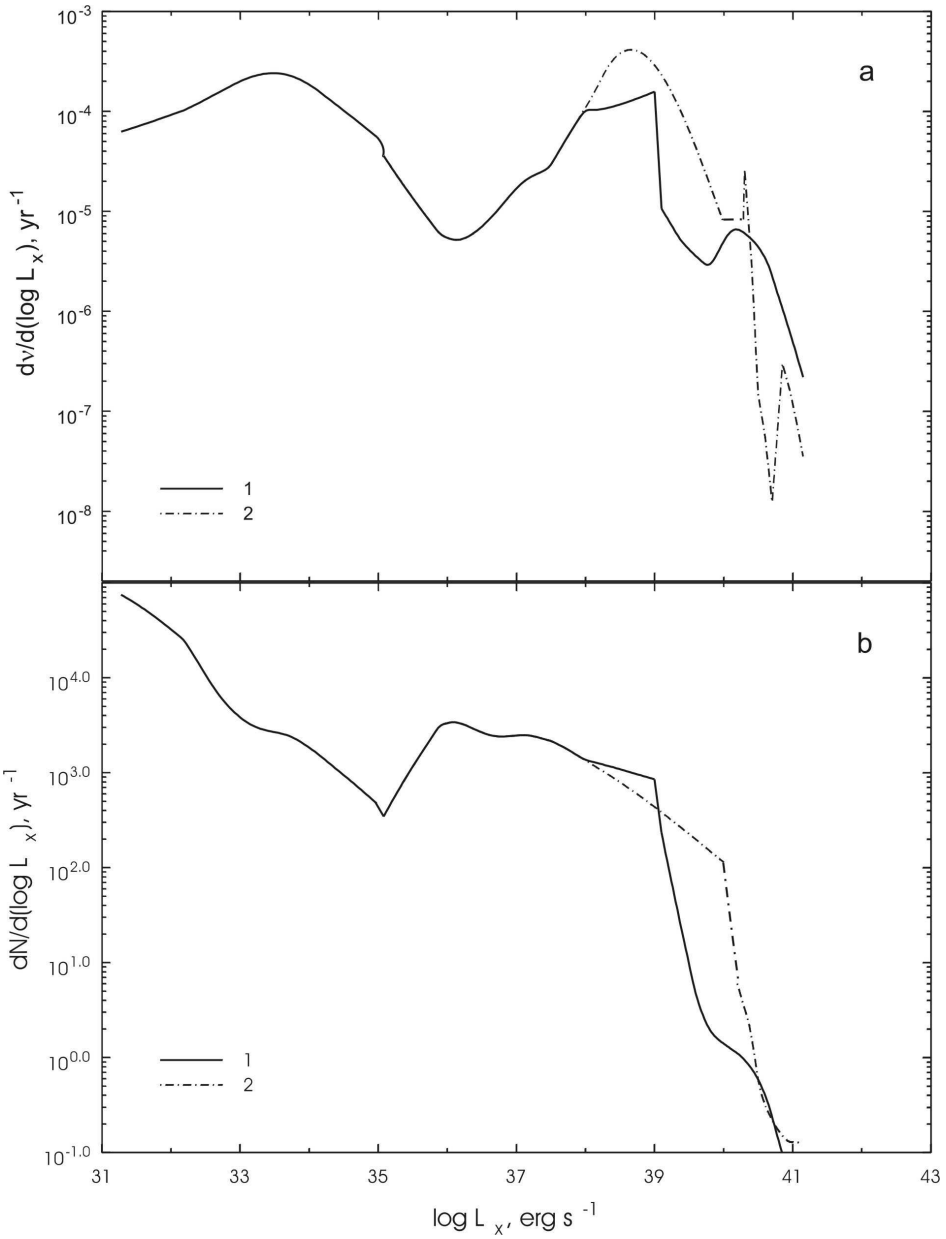

Fig. 11.— Birth frequency (a) of all investigated systems (differential function) and differential luminosity function (b) of X-ray binary sources in the Galaxy. Stellar wind type C. Marks in the Figure are: 1, collimation angle (for super critical regimes) $\alpha = 10°$; 2, $\alpha = 1°$.

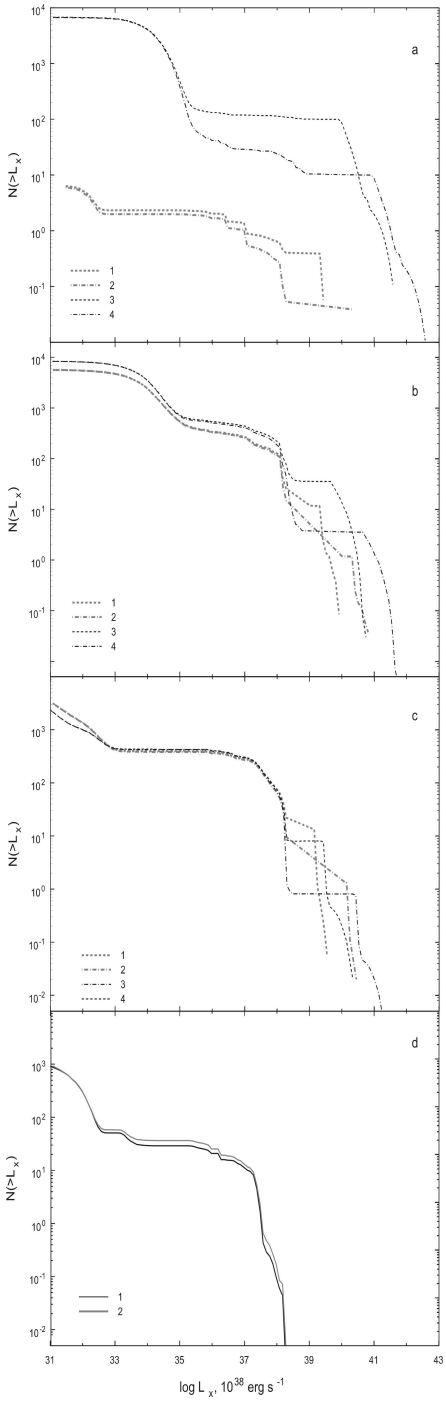

Fig. 12.— Cumulative luminosity functions of all investigated systems in the "elliptical" galaxy after the star formation burst. See Table 1 for numerical estimations. The curves in the Figure represent the next models: 1, stellar wind type A, collimation angle (for super critical regimes) $\alpha = 10°$; 2, wind A, $\alpha = 1°$; 3, wind C, $\alpha = 10°$; 4, wind C, $\alpha = 1°$. The time ranges after the star formation burst in the Figure are: a, 0-10 million years; b, 10-100 million years; c, 100 million – 1 billion years; d, 1-10 billion years.

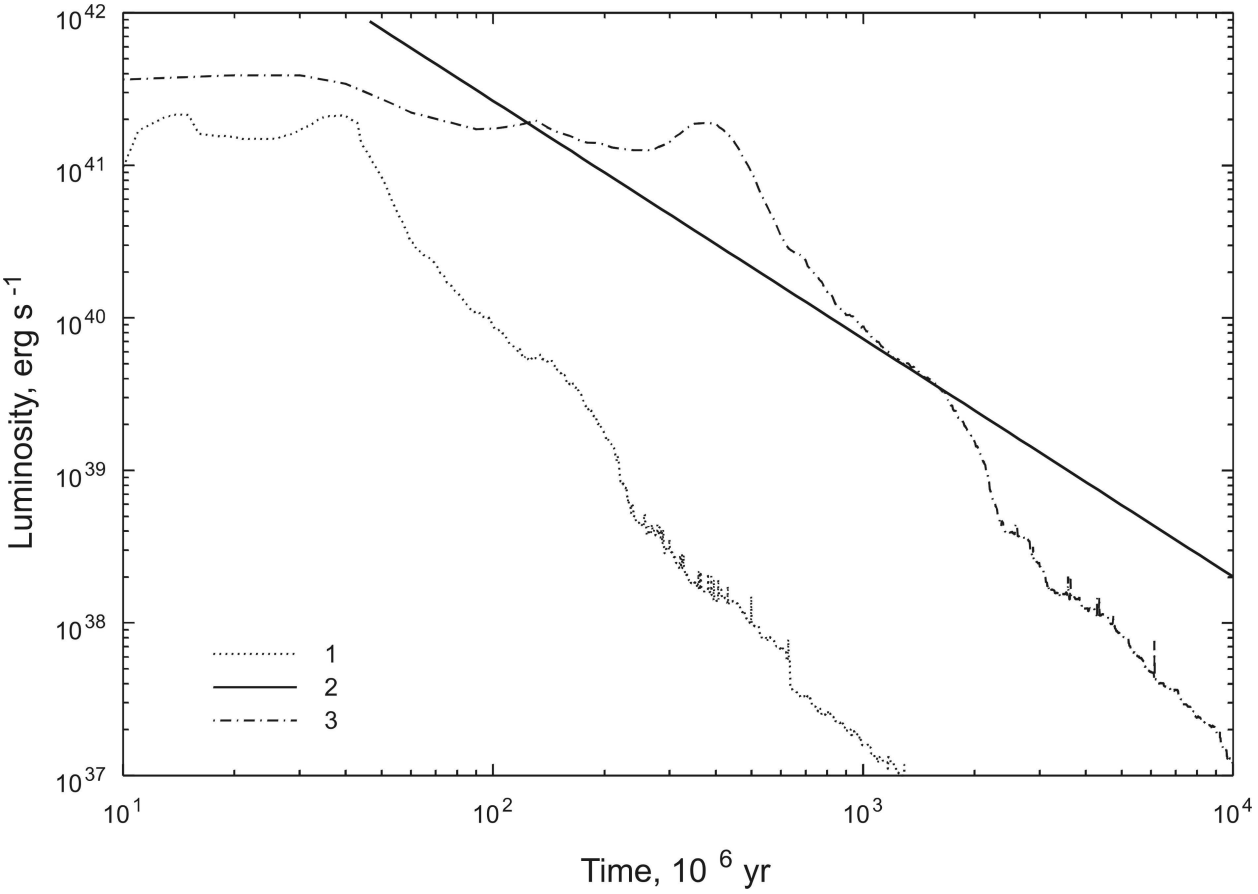

Fig. 13.— Evolution of the X-ray luminosity after the star formation burst ($T = 0$) in the galaxy with mass $10^{11} M_{\odot}$. See Table 2 for numerical data. In this Figure: 1, our calculations, stellar wind type A; 2, the result obtained by Tatarinzeva et al. (1989); 3, our calculations, stellar wind type C.

Table 1: Numerical approximation of the cumulative luminosity function in the spiral galaxy. Stellar wind type A. See Figure 8 for graphical data.

Luminosity range, $\log L_x$, erg s^{-1}	k[a]
31.0 – 32.5	-0.25
32.5 – 35.6	-0.1
35.6 – 37.2	-0.25
37.2 – 38.0	-0.7
38.0 – 38.3	≈ -8[b]
38.0 – 38.5	≈ -8[c]
38.3 – 39.2	≈ -0.05[b]
38.5 – 40.2	≈ -0.05[c]
39.2 – 41.1	-0.7[b]
40.2 – 42.2	-0.7[c]

[a] fit curve is $N(> L) \sim L^k$.

[b] collimation angle (for super critical regimes) $\alpha = 10°$.

[c] collimation angle (for super critical regimes) $\alpha = 1°$.

Table 2: Numerical approximation of the cumulative luminosity function in the spiral galaxy. Stellar wind type C. See Figure 9 for graphical data.

Luminosity range, $\log L_x$, erg s^{-1}	k[a]
31.0 – 32.5	-0.4
32.5 – 35.5	-0.1
35.5 – 37.2	-0.3
37.2 – 38.0	-0.6
38.0 – 38.2	-1.8[b]
38.0 – 38.2	-3.6[c]
38.2 – 39.1	-0.1[b]
38.2 – 40.1	-0.3[c]
39.1 – 39.5	-3.5[b]
40.1 – 40.5	-3.5[c]
39.5 – 41.0	-0.75[b]
40.5 – 42.0	-0.75[c]

[a] fit curve is $N(> L) \sim L^k$.

[b] collimation angle (for super critical regimes) $\alpha = 10°$.

[c] collimation angle (for super critical regimes) $\alpha = 1°$.

Table 3: Numerical approximation of the X-ray luminosity of the galaxy after the star formation burst. Stellar wind type A.

Time range, 10^6 yr	c_1 [a]	p [a]
$4 \cdot 10^2 - 1 \cdot 10^3$	$3 \cdot 10^{47}$	-2.5
$1 \cdot 10^3 - 2 \cdot 10^3$	$3.6 \cdot 10^{44}$	-1.56
$2 \cdot 10^3 - 2.5 \cdot 10^3$	$2 \cdot 10^{52}$	-4
$2.5 \cdot 10^3 - 1 \cdot 10^4$	$3 \cdot 10^{44}$	-1.8

[a] fit curve is $L(T) = c_1 (T/10^6 \mathrm{yr})^p$ erg s^{-1}.

Table 4: Numerical approximation of the X-ray luminosity of the galaxy after the star formation burst. Stellar wind type C.

Time range, 10^6 yr	c_1 [a]	p [a]
$4 \cdot 10 - 1 \cdot 40$	$1.5 \cdot 10^{41}$	≈ 0
$1 \cdot 40 - 1.5 \cdot 10^3$	$2 \cdot 10^{45}$	-2.7

[a] fit curve is $L(T) = c_1 (T/10^6 \mathrm{yr})^p$ erg s^{-1}.